VIP Heterogeneous Catalysis

DOI: 10.1002/ange.201105790

Observing Oxygen Storage and Release at Work during Cycling Redox Conditions: Synergies between Noble Metal and Oxide Promoter**

Mark A. Newton, Marco Di Michiel, Anna Kubacka, Ana Iglesias-Juez, and Marcos Fernández-García**

The ability of many materials to store and release gases lies at the core of a range of economically and environmentally important technologies.[1–6] To this end much research is directed towards developing materials that have an optimal storage capacity for the gases. However, in many cases, the implicitly "static" notion of "capacity" is only half the story. For practical operation gas uptake and release functions also need to be kinetically adapted to the process situation.[1,2]

The preeminent application that utilizes gas storage and release properties in a highly dynamic situation is three-way catalyst (TWC) operation for pollution abatement. Within this application TWCs have to respond to a rapidly alternating (1–2 Hz) redox environment.[3–7]

The principal role $CeZrO_4$ has within the TWC paradigm relates to the oxygen storage capacity (OSC). The OSC[7] ensures efficient conversion of CO and hydrocarbons into CO_2 in reducing conditions and of NO into N_2 at oxidizing conditions, even when the feedstock has become, respectively, diminished or enriched in oxygen with respect to a stoichiometric mixture.[4,6] $CeZrO_4$ has come to be seen as an optimal material for application in TWCs on the basis of its OSC properties and the increased thermal stability it bestows upon the catalyst system.[5] In spite of these considerations, only a few studies[8] have attempted to deal with the dynamic structural reactive aspects of its behavior. These studies have used extended X-ray absorption fine structure (EXAFS) spectroscopy at the cerium L_{III} and zirconium K edges to study a 1 wt% $Pt/CeZrO_4$ catalyst[8a] or environmental TEM to analyze the redox state of $CeZrO_4$ particles during reducing/oxidizing conditions.[8b]

Herein, we go further by coupling time-resolved hard (86.8 keV) X-ray diffraction (HXRD) or palladium K edge energy-dispersive EXAFS to diffuse reflectance infrared spectroscopy (DRIFTS) and mass spectrometry (MS).[9] This approach permits us to directly investigate the structure–activity relationship of the supported Pd nanoparticles, the nanoscale $CeZrO_4$ phases, and the adsorbates that are formed or converted over them, at the same time, and with subsecond time resolution. We therefore directly detect and kinetically quantify oxygen storage and release. Moreover, we elucidate several distinct facets to the synergetic interaction of the $CeZrO_4$ and Pd phases.

Figure 1 shows firstly (top left panel) on-line mass spectrometry pertaining to CO_2 production during alternate NO–CO–NO exposure at 673 K over two systems having similar Pd particle size (see the Supporting Information): 2 wt% Pd/Al_2O_3 (2PdA) and 4 wt% Pd/33 wt% $CeZrO_4/Al_2O_3$ (4Pd33ZCA) samples. This CO–NO single cycle is taken from within a larger experiment comprising 10 cycles as described previously.[9,10]

The color maps show HXRD data derived from 33ZCA and 4Pd33ZCA samples during CO/NO cycling at 673 K at

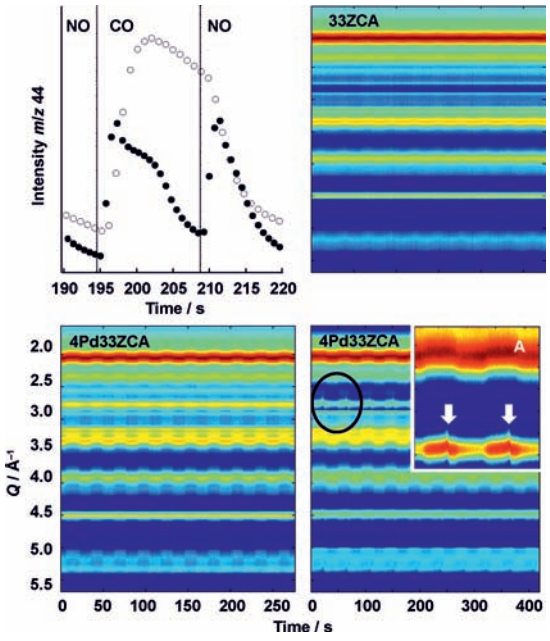

Figure 1. Temporal variation in m/z 44 (CO_2) observed for alternate NO–CO–NO exposure (13.86 s each gas) at 673 K over 2PdA (●) and 4Pd33ZCA (○) and variations in HXRD (color maps) observed during CO/NO cycling at 673 K over 33ZCA and 4Pd33ZCA samples and for cycling time between each gas of 13.86 s. The bottom right panel shows the result obtained for the 4Pd33ZCA at 673 K but with a gas exposure time of 21.41 s. The white arrows in the inset (A) highlight changes of d spacing in the Pd [111] reflection toward the end of the CO phase of the cycling.

[*] Dr. M. A. Newton, Dr. M. Di Michiel
European Synchrotron Radiation Facility
6, Rue Jules Horowitz, BP220, Grenoble, F-38043 (France)
E-mail: newton@esrf.fr
Dr. A. Kubacka, Dr. A. Iglesias-Juez, Prof. M. Fernández-García
Instituto de Catálisis y Petroleoquímica, CSIC, C/Marie Curie 2
28049, Madrid (Spain)
E-mail: mfg@icp.csic.es

[**] We thank the ESRF for access to facilities. Trevor Mairs, Pierre Van Vaerenbergh, Pascale Dideron, Dominique Rohlion, and Marchial Lambert are all gratefully thanked for their technical contributions to this work. Andy Fitch (ESRF) is also thanked for his advice regarding processing of the HXRD data.

Supporting information for this article, including experimental details, is available on the WWW under http://dx.doi.org/10.1002/anie.201105790.

a rate of 2 Hz per pattern.[9] For 4Pd33ZCA, two results are shown. The first was obtained using gas exposure periods of 13.86 s (each gas), the using second 21.41 s. The corresponding HXRD results obtained from a 2PdA sample along with Pd K edge dispersive EXAFS coupled to DRIFTS and MS for the 4Pd33ZCA system are given as Supporting Information.

In the 2PdA sample (see the Supporting Information),[9] CO_2 production is predominantly observed during the switching events. Although there is some further CO_2 production within the CO cycle itself, the overall efficiency of CO conversion is low during this period of the cycling. By contrast, over the 4Pd33ZCA a much higher level of CO_2 production is maintained throughout the reducing phase. These data show that the primary function of the $CeZrO_4$ phase (maintaining efficient CO conversion during lean operation) is successfully achieved under the model conditions applied. However, they do not establish how this superior catalytic efficiency is attained.

As recently shown by HXRD[9] (see also the Supporting Information) for the 2PdA sample, the lattice parameter of the Pd nanoparticles increases linearly during the CO exposure. In this case, the Pd nanoparticles respond to their environment by dissociating some of the adsorbed CO and then transiently storing atomic carbon within the nanoparticles. A return to the NO feed results in a rapid removal of this stored carbon, and the observed *d* spacing returns to that expected for fcc Pd nanoparticles.

The same experiment carried out over a 4Pd33ZCA sample reveals a quite different behavior. No evidence can now be found for the lattice parameter of the Pd nanoparticles changing during a 13.86 s CO exposure. Instead, it is the $CeZrO_4$ lattice parameter that constantly changes, albeit with a different temporal envelope, in response to the changing feed. It is now the $CeZrO_4$ phase that shoulders the structural-reactive strain applied by this model decontamination chemistry.

By using a 21.41 s period (Figure 1) over the 4Pd33ZCA sample, we observe a hybrid result. Up to a point we obtain a similar result to the shorter gas cycling time; that is, the lattice parameter of the $CeZrO_4$ phase oscillates while the Pd phase remains constant. However, toward the end of the extended CO exposure an abrupt change in behavior is observed, and the reflections arising from the Pd phase increase in intensity once again. Suddenly the system has started to behave as if the $CeZrO_4$ phase were not present.

Figure 2A shows the behavior of the 33ZCA and 4Pd33ZCA systems in more detail for a single (short, 13.86 s; see the Supporting Information for the 21.41 s run) CO–NO switching sequence. Here the relative change in *d* spacing of the Ce (222) reflection is plotted against time. In the absence of Pd, CO induces a linear expansion (1.0033 maximal relative change) of the $CeZrO_4$ lattice constant. In the presence of Pd, however, both the magnitude and the kinetic character of the change in *d* spacing of the $CeZrO_x$ phase changes significantly.

These data have been kinetically modeled using the approach of Avrami for isothermal processes [Eq. (1):][11]

$$\ln[-\ln(1-\alpha)] = n\ln(t) + n\ln(k) \quad (1)$$

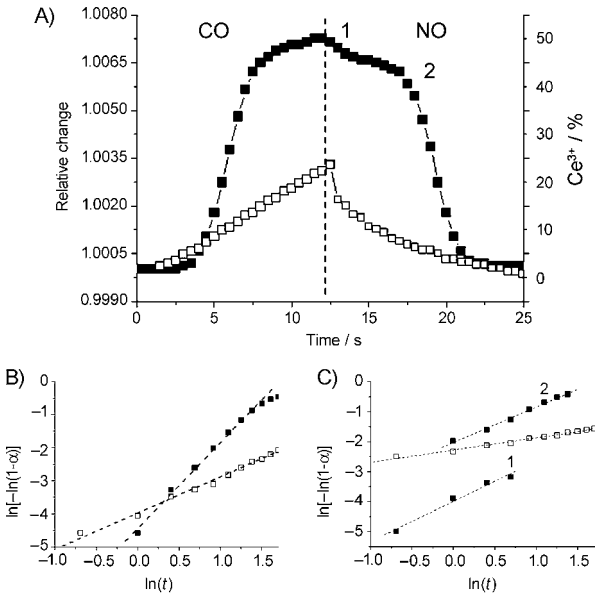

Figure 2. A) Relative change of the $CeZrO_4$ lattice constant and Ce^{3+} content during CO/NO cycling at 673 K for 33ZCA (□) and 4PdA33ZCA (■), during a single (13.86 s CO, 13.86 s NO) cycling period. B,C) The resulting Avrami analysis for the CO phase (B) and the subsequent NO exposure (C).

where α is the fraction of Ce^{3+} present at the material at time *t*, *k* is the temperature-dependent rate constant, and *n* is the Avrami exponent that describes how the transformation propagates through the material. Figure 2B,C shows the resulting double logarithmic $\ln\{-\ln(1-\alpha)\}$ versus $\ln(t)$ plots for the NO to CO (Figure 2B) and CO to NO switches (Figure 2C). Where an induction period (t_{ind}) appears to be present, *t* was replaced by $(t-t_{ind})$ in (1). In Figure 2A, this induction period is caused either by a chemical reaction between C- and N-containing fragments or gases at Pd surfaces (initial delay observed for 4Pd33ZCA in Ce^{3+} variations under CO) or by the existence of the preceding phenomena (e.g., 4Pd33ZCA under NO; the two phenomena marked as 1 and 2 in Figure 2). Table 1 summarizes the kinetic parameters (*n* and *k*) that arise from this analysis.

Table 1: Avrami exponent (*n*) and rate constant *k* (atoms of Ce min^{-1}) for the reduction and oxidation processes.

Cycle	Sample	*n*	*k*
CO	33ZCA	1.1	0.03
CO	4Pd33ZCA	2.6	0.018
NO	33ZCA	0.41	0.0003
NO	4Pd33ZCA	$1.3_1/1.2_2$	$0.05_1/0.178_2$

When considered together, the Pd K edge dispersive EXAFS (see the Supporting Information) and the HXRD tell very similar stories from complementary points of view. The structural variations that occur in the Pd nanoparticles are far greater in the absence of the 33ZCA phase than in its presence. Variations in the apparent average Pd K edge EXAFS coordination number (which most likely reflects

changes in particle shape and/or disorder) observed in the absence[9,10] of the $CeZrO_4$ are effectively curtailed in its presence (see the Supporting Information), as is the transient expansion of the Pd lattice, though as the longer CO exposure experiment shows, only up to a certain limit.

As such, the nanoscale contact of the $CeZrO_4$ phase with the Pd nanoparticles results in the latter being more robust (structurally speaking) in the face of the changing nature of the feed. Moreover, in the presence of $CeZrO_4$, and within a certain limit of CO exposure, the transient storage of atomic carbon arising from dissociation of CO by the Pd nanoparticles,[9] is completely curtailed. We can also see, by reference to measurements made on the Pd-free 33ZCA, that the contact of the Pd with the $CeZrO_4$ also has a profound promotional effect on the redox behavior of the oxide.

The source of the apparent "breathing" of the $CeZrO_4$ phase during the redox chemistry is the OSC function itself. The physical manifestation of this function has its origins in the considerable difference in size between Ce^{4+} and Ce^{3+}.[12–14] Loss of oxygen from $CeZrO_4$ promotes the formation of Ce^{3+}, causing a strain-induced swelling of the $CeZrO_4$ that is measured by the HXRD. This effect permits us to quantify the level of oxygen loss (or Ce^{3+} production) that these changes in lattice constant correspond to,[13–18] and therefore to access and quantify the kinetic character of the oxygen storage and release processes using the Avrami analyses (Figure 2).

These results show that while the $CeZrO_4$ phase donates its OSC to the overall operation of the catalyst, a considerable promotional synergy exists with the Pd as a result of the intimate contact of the two phases.[6,17,19] Starting at the CO step, Table 1 evidences a marked difference in the surface (e.g. $n \approx 1$) or tridimensional ($n \approx 3$) character of the reduction observed, respectively, for 33ZCA and 4Pd33ZCA samples.[11] The rate of reduction of the $CeZrO_4$ phase is also promoted by a factor six at 673 K (Table 1) in the presence of Pd. The relative magnitudes of these changes (see Figure 2) indicate that in the presence of the Pd, the $CeZrO_4$ phase oscillates between two states (e.g. roughly $Ce_2Zr_2O_{7.5}$ and $Ce_2Zr_2O_8$) equating to a maximum reduction of approximately 50% of the Ce ions.[18]

Re-oxidation, by NO, of the 33ZCA support oxidation appears to be diffusion-controlled ($n \approx 0.5$), a fact likely derived from site-blocking owing to the presence and decomposition of surface NO-derived species (typically hyponitrite).[6] The re-oxidation of 4Pd33ZCA initially resembles that of the support (Figure 2). The kinetic analysis nevertheless suggests a strong influence of Pd in the elimination of nitrogen-containing species present at the oxide surface. Table 1 suggests that the two oxidation steps observed upon NO treatment for 4Pd33ZCA have similar natures but with significantly different rates: the first from direct contact of NO-derived species with the oxide promoter; the second through Pd-activated oxygen species able to interact with the oxide promoter only after "cleansing" of the Pd particle surface.

We may also see that the proximity of the $CeZrO_4$ phase suppresses the dissolution of atomic carbon into the Pd particles up to a point. With a longer exposure to CO, however, we can also observe exactly when the OSC capacity of the $CeZrO_4$ becomes exhausted. Beyond this point, HXRD shows that carbon storage within the Pd phase recommences, thus demonstrating that oxygen transfer from the promoter oxide to the noble metal has ceased.

Thus HXRD allows us to discriminate between two sources of the suppression of the PdC_x phases by $CeZrO_4$. Firstly, the contact of $CeZrO_4$ with the Pd nanoparticles might pacify them, such that CO is no longer dissociated; or, secondly, CO dissociation still occurs over the Pd, but as long as oxygen transfer from the $CeZrO_4$ is active, the resulting atomic carbon is efficiently shepherded back into the CO oxidation process by the oxygen release from the $CeZrO_4$. If this process stops, atomic carbon may once again be free to dissolve into the Pd particles. The HXRD evidence strongly suggests it is the latter explanation that is at work in this case.

What, however, is the effect of the presence of $CeZrO_4$, and the modifications to the structural behavior of the Pd that it induces, on the surface molecular speciation during this model decontamination catalysis? To answer this question, we turn to the synchronously collected DRIFTS data. Figure 3 shows results derived from the time-resolved DRIFTS, again for alternate NO–CO–NO exposure, and for

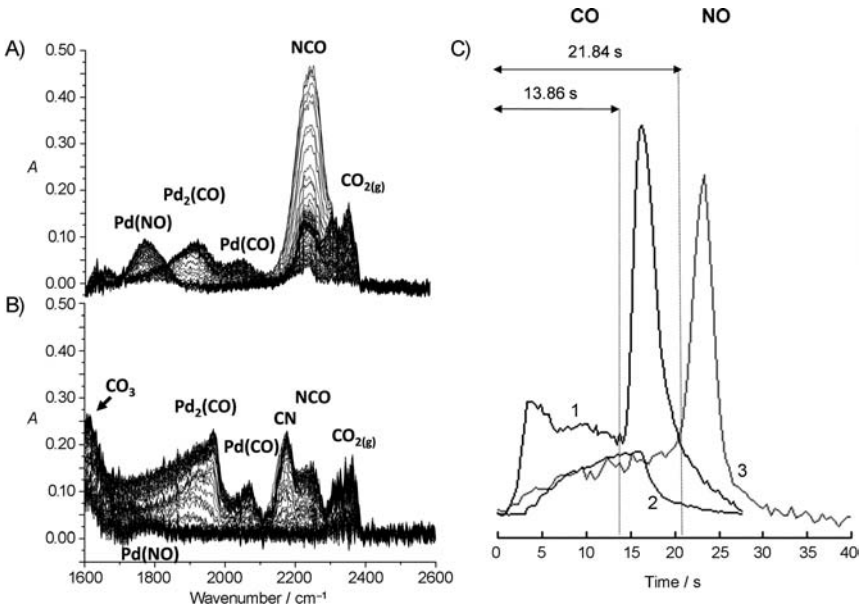

Figure 3. Background-subtracted DRIFTS spectra at 673 K and during the CO part (13.86 s) of the cycle over A) 2PdA and B) 4Pd33ZCA samples. C) Temporal behavior of the IR band arising from adsorbed NCO species (2240 cm^{-1}) from 2PdA (1), 4Pd33ZCA (2, 13.86 s CO exposure), and 4Pd33ZCA (3, 21.41 s exposure to CO). Though not shown, the CN band (observed only for 4Pd33ZCA) shows the same temporal envelope.

both 2PdA (Figure 3 A) and 4Pd33ZCA samples (Figure 3 B) during CO/NO cycling (13.86 s exposure per gas) at 673 K. Figure 3 C) shows the temporal variation of adsorbed NCO species in each case along with that observed for the extended (21.41 s) CO exposure. Further IR observables are given in the Supporting Information.

Six modifications to the molecular speciation, resulting from the presence of the $CeZrO_4$/Pd contact, can be observed: 1) elevated levels of carbonate species (below 1700 cm^{-1}) in the presence of $CeZrO_4$; 2) a large suppression of molecular NO species (ca. 1780 cm^{-1}); 3) a drastic curtailment of the maximum level of NCO formation at the switch from CO back to NO in the shorter of the two cycling periods; 4) the appearance of a new species (2175 cm^{-1}), assigned as Pd–CN;[17] 5) a significant blue shift, and changes in the shape of the band due to bridging CO species, and a smaller blue shift in the frequency of the linear CO band adsorbed upon the Pd; and lastly, 6) a highly significant change in the absolute values and temporal dependence of the bridge-to-linear (B/L) CO ratio (detailed in the Supporting Information).

Some of these changes can be directly associated with products of CO dissociation or the suppression of the formation of PdC_x phases by the $CeZrO_4$. Others we might assign to either electronic or interfacial effects arising directly out of the intimate contact between the Pd and $CeZrO_4$ phases.

Taking the former cases first, the appearance of Pd–CN (2175 cm^{-1}) indicates a differential behavior of the NCO species, the likely precursor of CN.[17] As the Pd has a similar particle size in the 2PdA and 4Pd33ZCA samples, this difference points to a $CeZrO_4$ role when in contact with the metal. A direct role of the OSC, in storing oxygen from the NCO molecule, is therefore implied.

The very significant change in the carbonyl bridge/linear ratio (B/L; see the Supporting Information) is also linked to the suppression of PdC_x formation by the $CeZrO_4$. The formation of the PdC_x phase promotes the formation of linear CO.[9] A suppression of PdC_x formation in the presence of $CeZrO_4$ should therefore result in higher B/L ratios that remain constant once an equilibrium CO coverage is achieved, as is observed. However, it is only the simultaneous application of the HXRD and DRIFTS that allows this relationship to be unequivocally established.

The overall changes in behavior of the NCO species during this chemistry can also be linked to the formation, or lack thereof, of PdC_x during the CO cycle. This species is much more abundant at the switch from CO to NO in the 2PdA than the 4Pd33ZCA case when the CO exposure is kept short enough. The latter observation implies that this latter burst of NCO production draws, at least in part, from the reservoir of atomic C present within the Pd nanoparticles in the 2PdA case. As no such reservoir exists in the presence of $CeZrO_4$ after this length of CO exposure (13.86 s), this pathway for NCO formation no longer exists. This hypothesis is verified by the reappearance of this large burst of NCO formation after the extended exposure to CO (21.41 s) and after the OSC of the $CeZrO_4$ has been shown (by HXRD) to have been exhausted.

Of the other observations, that of a very much diminished population of molecular NO species in the presence of the $CeZrO_4$ is the most significant from a process perspective, yet it is not obviously associable with any of the dynamic structural changes revealed by the X-ray probes. We link this diminished population, therefore, to either the formation of new Pd/$CeZrO_4$ interfaces and/or electronic perturbation of the Pd. As the size of the Pd nanoparticles would appear to be similar in both 2PdA and 4Pd33ZCA (see the Supporting Information), this difference cannot easily be ascribed to size dependencies in NO dissociation by the Pd nanoclusters. This conclusionwould be consistent with previous studies, which have pointed to an absence of such size-effects in this size regime.[20] The considerable reduction in levels of molecular NO species observed in the presence of the $CeZrO_4$ indicates that one of the effects of the intimate oxide/metal contact is a significant promotion of NO dissociation by Pd. Indeed, this is a key step for efficient conversion of NO to N_2 and the primary reason for which Rh has been historically included in the formulation of TWCs.[4,6,21]

In summary, by combining HXRD, EXAFS, DRIFTS, and MS measurements,[22] we have observed and quantified, in real time, the oxygen storage and release functions of nanosized $CeZrO_4$. This approach uncovers the sources of several behavioral traits fundamental to the exceptional performance of TWCs. These traits arise from the intimate contact of the Pd with the $CeZrO_4$ phase and must come together to yield an enhanced applied behavior. The multifacetted structural role of the $CeZrO_4$ phase can be summarized as firstly, significantly increasing Pd dispersion for a given loading;[17b] secondly, inducing an increased resistance of the Pd nanoparticles to structural change (shape and disorder) in the face of the changing redox potential of the feed; and, thirdly, suppressing the formation of PdC_x phases during the CO cycle through efficient oxygen release, although HXRD and IR spectroscopy show that CO dissociation is still occurring. The OSC function of the $CeZrO_4$ effectively reintegrates much of the "lost" atomic carbon species back into the overall CO oxidation process within the reducing cycle. Importantly, we have also shown that intimate nanoscale contact with Pd nanoparticles results in a significant reverse synergy; one that promotes oxygen storage and release. Lastly we have gained evidence for further electronic perturbation that arises from the presence of $CeZrO_4$; one that promotes a fundamental step—dissociative NO adsorption.

Received: August 16, 2011
Published online: October 20, 2011

Keywords: cerium oxide · heterogeneous catalysis · palladium · structure–activity relationships · X-ray absorption spectroscopy

[1] For H_2, see, for example: J. Yang, A. Sudik, C. Wolverton, D. J. Siegel, *Chem. Soc. Rev.* **2010**, *39*, 656–675.

[2] a) For storage sequestration and release of CH_4, H_2, and CO_2 using Clathrate hydrates, see, for example: A. K. Sum, C. A. Koh, E. D. Sloan, *Ind. Eng. Chem.* **2009**, *48*, 7457–7465; b) for H_2 or CO_2 storage and release on MOFs, see, for example:

J. L. C. Rowsell, O. M. Yaghi, *Microporous Mesoporous Mater.* **2004**, *73*, 3 – 14.
[3] For NO_x storage and reduction, see, for example: S. Roy, A. Baiker, *Chem. Rev.* **2009**, *109*, 4054 – 4091.
[4] E. S. J. Lox, B. H. Lengler, *Environmental catalysis* (Eds.: G. Ertl, H. Knozinger, H. J. Weitkamp), Wiley-VCH, Weinheim, **1999**, p. 1.
[5] R. Di Monte, J. Kaspar, *J. Mater. Chem.* **2005**, *15*, 633 – 648.
[6] A. Martinez-Arias, J. C. Conesa, M. Fernandez-Garcia, J. A. Anderson in *Supported Metals in Catalysis*, (Eds.: J. A. Anderson, M. Fernandez-Garcia), Imperial College Press, London, **2005**, pp. 283 – 326.
[7] M. Sugiura, M. Ozawa, A. Suda, T. Suzuki, T. Kanasawa, *Bull. Chem. Soc. Jpn.* **2005**, *78*, 752 – 767.
[8] a) T. Yamamoto, A. Suzuki, Y. Nagai, T. Tanabe, F. Dong, Y. Inada, M. Nomura, M. Tada, Y. Iwasawa, *Angew. Chem.* **2007**, *119*, 9413 – 9416; *Angew. Chem. Int. Ed.* **2007**, *46*, 9253 – 9256; b) R. Wang, P. A. Crozier, R. Sharma, J. B. Adams, *Nano Lett.* **2008**, *8*, 962 – 967.
[9] M. A. Newton, M. Di Michiel, A. Kubacka, M Fernández-García, *J. Am. Chem. Soc.* **2010**, *132*, 4540 – 4541.
[10] M. A. Newton, C. Belver-Coldeira, A. Martínez-Arias, M. Fernández-García, *Nat. Mater.* **2007**, *6*, 528 – 532.
[11] a) M. Avrami, *J. Phys. Chem.* **1940**, *8*, 212 – 218; b) J. L. Allen, T. R. Jow, J. Wolfenstine, *Chem. Mater.* **2007**, *19*, 2108 – 2111; c) E. E. Finney, R. G. Finke, *Chem. Mater.* **2009**, *21*, 4692 – 4705.
[12] See, for example: http://www.webelements.com.
[13] M. Morgensen in *Catalysis by Ceria and Related Materials* (Ed.: A. Trovarelli), Imperial College Press, London, **2002**, pp. 453 – 482.
[14] S. Nagabhusan Achary, S. K. Sali, N. K. Kulkarni, P. S. R. Krishna, A. B. Shinde, A. K. Tyagi, *Chem. Mater.* **2009**, *21*, 5848 – 5859.
[15] J. A. Rodriguez, J. C. Hanson, J.-Y. Kim, G. Liu, A. Iglesias-Juez, M. Fernández-García, *J. Phys. Chem. B* **2003**, *107*, 3535 – 3543.
[16] M. Fernández-García, X. Wang, C. Belver, A. Iglesias-Juez, J. C. Hanson, J. A. Rodriguez, *Chem. Mater.* **2005**, *17*, 4181 – 4193.
[17] a) S. Kameda, T. Chafit, Y. Ukisu, T. Miyadera, *Catal. Lett.* **1998**, *55*, 211 – 214; b) A. Iglesias-Juez, A. Martínez-Arias, M. Fernández-García, *J. Catal.* **2004**, *221*, 148 – 161.
[18] S. N. Achary, S. K. Sali, N. K. Kulkarni, P. S. R. Krishna, A. B. Shinde, A. K. Tyagi, *Chem. Mater.* **2009**, *21*, 5848 – 5859.
[19] G. N. Vayssilov, Y. Lykhach, A. Migani, T. Staudt, G. P. Petrova, N. Tsud, T. Skála, A. Bruix, F. Illas, K. C. Prince, V. Matolín, K. M. Neyman, J. Libuda, *Nat. Mater.* **2011**, *10*, 310 – 315.
[20] A. Kubacka, A. Martínez-Arias, M. Fernández-García, M. Di Michiel, M. A. Newton, *J. Catal.* **2010**, *270*, 275 – 284.
[21] See, for example: M. Shelef, G. W. Graham, *Catal. Rev. Sci. Eng.* **1994**, *36*, 433 – 457.
[22] M. A. Newton, *Top. Catal.* **2009**, *52*, 1410 – 1424.

